Journal of Magnetism and Magnetic Materials 409 (2016) 111–115

Contents lists available at ScienceDirect

Journal of Magnetism and Magnetic Materials

journal homepage: www.elsevier.com/locate/jmmm

Structural and magnetic properties of manganese zinc ferrite nanoparticles prepared by solution combustion method using mixture of fuels

V. Jagadeesha Angadi [a], B.Rudraswamy [a], K. Sadhana [b], K.Praveena [c,*]

[a] Department of Physics, Bangalore University, Bangalore 560056, India
[b] Department of Physics, University College of Science, Osmania University, Saifabad, Hyderabad 500004, India
[c] School of Physics, Eternal University, Baru Sahib 173101, Himachal Pradesh, India

ARTICLE INFO

Article history:
Received 26 November 2015
Received in revised form
20 February 2016
Accepted 29 February 2016
Available online 2 March 2016

Keywords:
Ferrites
Complex permeability
Saturation magnetization
Magneton number

ABSTRACT

The structural analysis and magnetic investigation $Mn_{1-x}Zn_xFe_2O_4$ with stoichiometry ($x=0$, 0.1, 0.3, 0.5, 0.7, 0.9 and 1.0) were synthesized by solution combustion method using mixture of fuel this is first of its kind. As synthesized Mn–Zn nanoferrites were characterized by X-ray Diffractometer (XRD), Transmission electron microscopy (TEM) at room temperature. The magnetic domain relaxation was investigated by inductance spectroscopy (IS) and the observed magnetic domain relaxation frequency (f_r) was increased with the increase in grain size. The Room temperature magnetic properties were studied using vibrating sample magnetometer (VSM). It was observed that the real and imaginary part of permeability (μ' and μ''), saturation magnetization (M_s), remanance magnetization (M_r) and magneton number (M_r/M_s) were decreases gradually with increasing Zn^{2+} concentration. The decrease in the saturation magnetization may be explained as, the Zn^{2+} concentration increases the relative number of ferric ions on the A sites diminishes and this reduces the A–B interaction. Hence synthesized materials are good for high frequency applications.

1. Introduction

Ferrimagnetic materials mainly composed of iron oxide called ferrites. Ferrites having a spinel cubic structure and the general formula is AB_2O_4, where A is a divalent metal ion(Mn^{2+}, Zn^{2+}, Ni^{2+}, Cu^{2+}, Mg^{2+}) and B is the trivalent metal ions (Fe^{3+}, Cr^{3+}, Sc^{3+}, Sm^{3+}, Gd^{3+}). The spinel configuration is based on a face centered cubic (fcc) lattice of oxygen ions, forming tetrahedral (A) and octahedral (B) sites that may be occupied either by A and/or B site. In normal, the transition metal ion having valency 2+ occupy the tetrahedral sites and transition or rare earth ions having valency 3+ occupy the octahedral sites. If divalent metal ions occupy the octahedral sites and trivalent ions are distributed among tetra and octahedral sites. Based on the occupancy of the metal ions the ferrite materials exhibit excellent properties such as structural, electrical and magnetic properties. Among all the ferrites Mn–Zn ferrites possess excellent properties because they having high electrical resistivity, high saturation magnetization, high permeability and low power loss hence they are attracted to high frequency applications [1–3]. The Mn–Zn ferrites are magnetic oxide materials with semiconducting nature which are of great technological importance. The general important application of Mn–Zn ferrite materials used in transformer cores, antenna rods, memory chips, high density magnetic recording media, permanent magnets, transducers, activators microwave and computer technology etc. [4–6]. Furthermore, researchers using several methods to synthesis nanoferrites such as ball milling method [7], co precipitation method [8], hydrothermal method [9] and auto combustion method [10,11]. However Among these methods, the solution combustion method is a facile approach with great economic and technical advantages to obtain highly crystalline nanoparticles [7]. In the present investigation we adopt solution combustion method to synthesize Mn–Zn nanoferrite particles using urea and glucose as a mixed fuels. The first time Mn–Zn ferrites were synthesized solution combustion method using mixture of fuel. Furthermore, the substitution of Zn^{2+} at A-site shows decrees in structural as well as magnetic properties in $MnFe_2O_4$. This motivates us to synthesize the Zn^{2+} substituted $MnFe_2O_4$ nanoparticles and detailed investigation on structural and magnetic properties.

* Corresponding author.
E-mail address: praveenaou@gmail.com (K. Praveena).

http://dx.doi.org/10.1016/j.jmmm.2016.02.096
0304-8853/

2. Experimental

The nanocrystalline $Mn_{(1-x)}Zn_xFe_2O_4$ (x=0, 0.1, 0.3, 0.5, 0.7, 0.9 and 1.0) were prepared by solution combustion using urea and glucose as a fuel. The stiochiometric molar amounts of manganese nitrate [Mn $(NO_3)_2{\cdot}4H_2O$], zinc nitrate [Zn $(NO_3)_2{\cdot}6H_2O$], and iron nitrate [Fe $(NO_3)_3{\cdot}9H_2O$] as oxidizer and mixture of urea [NH_2CONH_2] and glucose [$C_6H_{12}O_6$] as a fuels. The Stiochiometric compositions of metal nitrates and fuels were evaluated based on the total oxidizing and reducing valences of the components and the oxidizer to fuel ratio was taken as 1: (60:40). All the metal nitrates and fuels were diluted with 30 ml double distilled water and thoroughly mixed with the help of magnetic stirrer with the speed of 800 rpm for one hour until the reactants were dissolved completely to get homogenous solution. This homogeneous solution containing redox mixture was taken in a Pyrex dish and kept in a pre-heated muffle furnace maintained at 450 ± 10 °C.

In the combustion synthesis, besides the target product (Mn–Zn ferrite), gases in the most stable form, i.e., CO_2, H_2O, and N_2, are produced as gel is being combusted. Carbon and hydrogen with a valence of 4+ and 1+, respectively, are regarded as reducing agents, oxygen with a valence of 2− is regarded as an oxidizing agent and the valence of nitrogen amounts to zero. The stoichiometric redox reaction for the systems in which O/F=1 according to the proposed equations:

Fuel: Mixture of fuel (60:40) urea [NH_2CONH_2] and glucose [$C_6H_{12}O_6$]

$$17(1-X)Mn(NO_3)_2 4H_2O + 17(X)Zn(NO_3)_2 6H_2O + 34Fe(NO_3)_3 9H_2O + 30NH_2CONH_2 + 20C_6H_{12}O_6 + (12-17X)O_2 = 17Mn_{1-X}Zn_XFe_2O_4 + 150CO_2 + 98N_2 + (55 + 34X)H_2O \quad (1)$$

Initially, the solution boils then froths and ignites to yield fine powder of Mn–Zn rapidly because these are exothermic. The whole combustion process was complete in less than 20 min, whereas the reaction time of the actual ignition was less than 5 s. The formation of Mn–Zn ferrite was possible due to the gas phase reaction between decomposition products of metal nitrates (nitrogen oxides) and fuels. The obtained powder was pressed in to the cylindrical pellets by applying the pressure of 5-ton/cm^2 for 5 min and sintered at 1000 °C/2 h in muffle furnace.

The sintered pellet were characterized by X-ray Diffractometer with CuK_α radiation (λ=0.154056 nm). Transition electron microscopy (TEM) and magnetization was carried out by vibrating sample magnetometer (VSM) mounted on an electromagnet with a bipolar source of maximum applied field of 1.5 T at room temperature.

3. Results and discussion

3.1. Structural analysis

Fig. 1 shows the room temperature X-ray diffraction patterns of all the samples of $Mn_{1-x}Zn_xFe_2O_4$ nanoferrites and it confirms the spinal cubic structure with space group ***Fd3m*** (Oh7) for all the composition. The broad diffraction peaks indicates that the ferrite particles are of Nano-sized. It is also observed that the presences of secondary phases in the XRD pattern of some compositions (M3, M4, M5, and M6) of the 2θ is around 34° is identified as α-Fe_2O_3 and the amount of this phase is found to be very small and it has

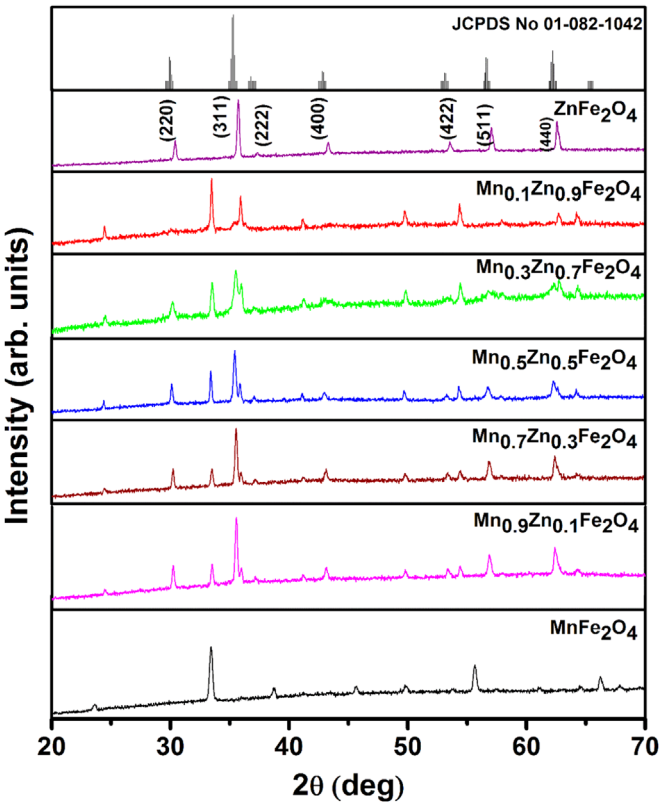

Fig. 1. X-ray diffraction patterns of $Mn_{1-x}Zn_xFe_2O_4$ (x=0, 0.1, 0.3, 0.5, 0.7, 0.9 and 1.0) sintered at 1273 K at 2 h.

no effect on the electrical and magnetic properties of present ferrites [12]. The average crystallite size of the each composition was calculated from the line width of the (3 1 1) peak of XRD pattern using the Scherrer formula [12].

$$t = \frac{0.9\lambda}{\beta \cos\theta}\ \text{nm} \quad (2)$$

where 't' is crystallite size, 'λ' is wavelength of X-ray radiation, 'θ' is Bragg's angle, is full width at halfmaximum. The structural parameters such as average crystallite size, cell volume and lattice parameter are varies with Zn^{2+} concentration increases. The average particle size of all the composition varies in the range of 25–35 nm. The lattice parameter and cell volume is decrease with increasing Zn^{2+} content. The decrease of lattice parameter and cell volume is due to the larger ionic radius Mn^{2+} ions (~0.091 nm) replaced by smaller ionic radius of Zn^{2+} ions (~0.082 nm) [13]. The value of lattice parameter and cell volume is listed in Table 1.

The distances between the magnetic ions at tetrahedral (A) and octahedral (B) sites were calculated by using the following equation.

$$L_A = a\frac{\sqrt{3}}{4} \text{ and } L_B = a\frac{\sqrt{3}}{2} \quad (3)$$

The variation of hopping length of tetrahedral site (L_A) and octahedral site (L_B) is as shown in the Fig. 2(a) and (b). Both the hopping length of L_A and L_B decreases with increasing Zn concentration. This may be cause of due to the decreases in lattice parameter of all the samples of increasing Zn^{2+} concentration.

3.2. Transition electron microscopy

Fig. 3(a) and (b) illustrates the TEM images of samples of composition x=0.0, 0.3. The particle sizes were analyzed using

Table 1
Data of Lattice parameter, Saturation magnetization (M_s) remanance magnetization (M_r), coercivity (H_c),remanance ratio (M_r/M_s), magneton number (n_B) for $Mn_{1-x}Zn_x Fe_2O_4$ nanoferrites at 300 K.

Composition (x)	Lattice parameter (nm)	Average Particle Size by TEM (nm)	Saturation Magnetization (M_s) Am^2/kg	Remanence magnetization (M_r) Am^2/kg	Coercivity (H_c) (T)	M_r/M_s	Magneton number (n_B)
0.0	0.8432	25	71.75	29.11	0.01631	0.405	2.469
0.1	0.8430	28	64.62	26.25	0.01645	0.406	2.223
0.3	0.8407	29	53.2	20.54	0.01663	0.387	1.824
0.5	0.8399	32	50.67	21.46	0.01677	0.423	1.743
0.7	0.8389	33	41.73	16.95	0.01639	0.406	1.435
0.9	0.8384	35	35.31	14.25	0.01635	0.404	1.215
1.0	0.8372	35	10.73	4.349	0.01644	0.405	0.394

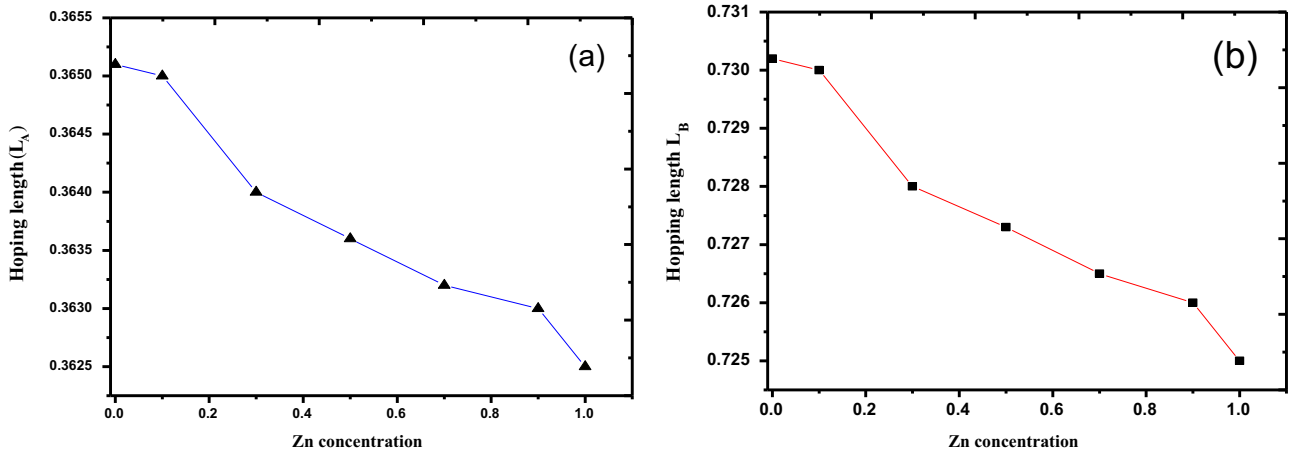

Fig. 2. (a–b) Variation of hopping length (L_A and L_B) with composition x for the system $Mn_{1-x}Zn_xFe_2O_4$.

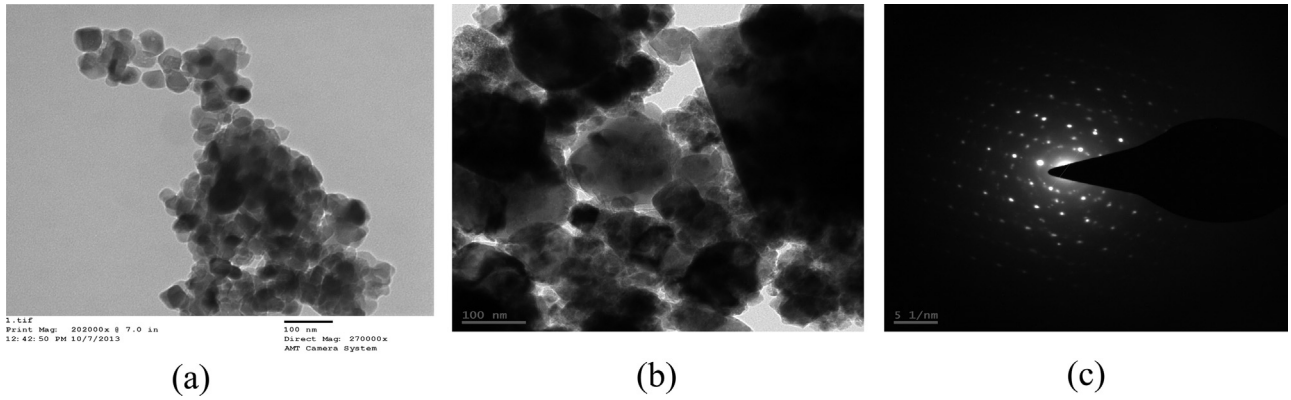

Fig. 3. TEM image of (a) $MnFe_2O_4$ (b) $Mn_{0.5}Zn_{0.5}Fe_2O_4$ (c) SAED pattern of $Mn_{0.5}Zn_{0.5}Fe_2O_4$.

ImageJ1.46r software. The images show cubic particles with less regularity in size and shape. The particles are agglomerated due to their slow growth of particles during the preparation method [14]. The estimated average size of the particle was about 25–35 nm. The particle size obtained from Transmission electron microscopies are in agreements with the average crystallite size calculated by Scherer formula using XRD data. Fig. 3(c) shows a selected area electronic diffraction (SAED) pattern of $Mn_{0.5}Zn_{0.5}Fe_2O_4$.The Electron Diffraction pattern consists of concentric rings with spots over the rings, this feature indicates that the samples are in crystalline in nature.

3.3. Magnetic properties

Fig. 4 shows the magnetic hysteresis curves of the samples investigated at room temperature. It very narrow hysteresis loops were observed and hence synthesized materials are soft magnetic material. This feature of Mn–Zn ferrites indicates that presence of superparamagnetic and single- domain particles for each of these ferrites [15]. From Table 1, it is found that the values of saturation magnetization (M_S), remnant magnetization (M_r), remnant ratio (M_r /M_s), coercivity (H_c) and magneton number (n_B) are found to be decreasing with increasing in Zn^{2+} concentration. According to Neel's two sub-lattice model of ferrimagnetism, the net moment is given by the formula $\mu th = M_B(x) - M_A(x)$, where M_A and M_B are the A and B sub-lattice magnetic moments [16]. The existence of random canting of particle surface spins; surface effects and the occurrence of a glassy state have been reported to be playing an active role in the decline of magnetization values [17]. As the zinc concentration increases, Fe^{3+} ions migrate from octahedral (B site) to tetrahedral (A site) and Mn^{2+} concentration decreases from both tetrahedral (A site) and octahedral (A site). Therefore, the magnetization of the B-site decreases while that of A-site increases the results in decrease in net magnetization

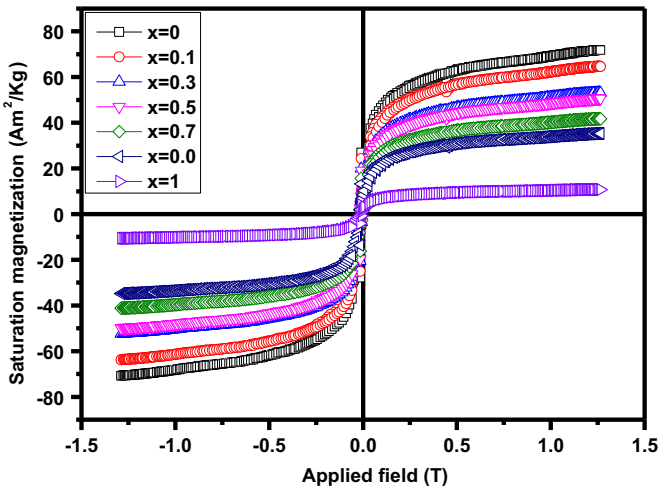

Fig. 4. Room temperature *M–H* curves for $Mn_{1-x}Zn_xFe_2O_4$ (x=0.0, 0.1, 0.3, 0.5, 0.7, 0.9, and 1.0).

In case of ferrite nanoparticles of the series $Mn_{1-x}Zn_xFe_2O_4$ were found to be showing reduced magnetization [18]. The respective reduction in magnetization may be due to a rearrangement of cations because of the changed preferential occupancy in the case of nanosized ferrites that is a change in distribution of Mn^{2+} and Zn^{2+} on the two sites. Zinc ferrite is a normal spinel and has no magnetic moment. Manganese ferrite is an inverse spinel and consequently, the two magnetic sub lattices are antiferromagnetically aligned. When the nonmagnetic zinc ion is substituted for manganese ferrite lattice, it has stronger preference for the tetrahedral site (A-site) than does the ferric ion and thus reduces the amount of Fe^{3+} ions on the A-site. Because of the antiferromagnetic coupling, the result is an increase in magnetic moment on the octahedral site (B-site) and an increase in the saturation magnetization [19].

However, the lower magnitudes of magnetization and occurrence of a net magnetic moment of the order of 10.73 A m^2/kg in zinc ferrite (for x=1) at room temperature is indicative of the presence of Zn^{2+} ions on the octahedral sites in nanoregime. It can alter the cation distribution to a greater extent which is deciding factor in determining the overall magnetic properties in the nanoregime. The magnetic moments of $Mn^{2+}/Fe^{3+}$and Mn^{3+}/Fe^{2+} ions are 5 and 4μ_B respectively. Hence the presence of Mn^{3+}/Fe^{2+} pairs in the B lattice reduces the net magnetic moment of the octahedral lattice, which will create a decline in the net magnetization. The presence of Mn^{3+} and Fe^{2+} in octahedral site leads to Jahn–Teller distortion which affects the magnetic properties in manganese containing ferrite [20].

In ferrites, the coercive force is obtained by the reversal of directions of the wall movement and that of domain rotation by reversing the direction of the applied magnetic field. Generally, the effective pinning for domain wall causes the coercivity, it is known that the larger grain size decreases H_C. In the present investigation, the coercive values are low hence probability of domain rotation is also lower. The materials with larger grain size have been used to achieve lower core loss [21]. With increase of Zn^{2+} content, the coercivity of all the samples were as small as $\sim$0.0165 $\pm$ 3 T, which indicates the super paramagnetic nature of the particles in the compositions

The real and imaginary parts permeability (μ' and μ'') represents the storage capability and loss of magnetic energy [22] is as shown in Fig. 5(a) and (b). In general, the performance of Mn–Zn ferrites can be estimated from the studies of frequency dependent on permeability. From the figure, the real part of permeability is found to remain constant up to 100 MHz and then rise

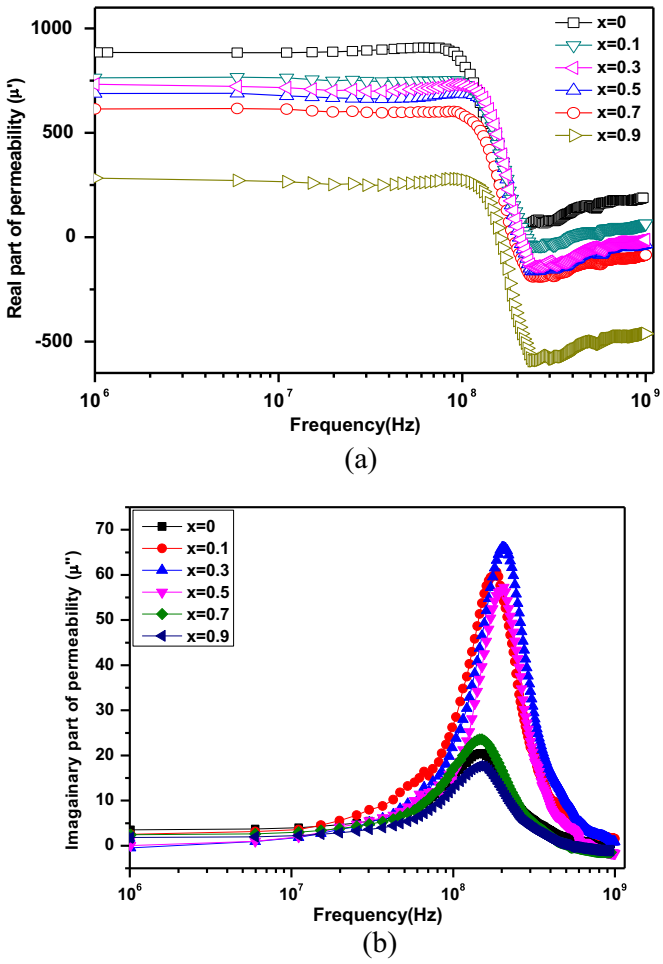

Fig. 5. Frequency dependence of (a) real part of permeability and (b) imaginary part of permeability for $Mn_{1-x}Zn_xFe_2O_4$ (x=0.0, 0.1, 0.3, 0.5, 0.7, 0.9, and 1.0).

to a maximum before falling rapidly to low values due to ferromagnetic resonance. The flat region up to where it starts decreasing rapidly indicates the compositional dependence quality of ferrites [23]. For the use of Mn–Zn ferrites in broadband and pulse transformers and wide band read/write heads for high definition video recording devices, the real part permeability should remain fairly constant over certain frequency ranges. The maximum of real part of permeability was obtained around 800 MHz. The negative values beyond resonance indicate that the relaxation effect which is not pronounced over such frequencies [24]. The dispersion of real permeability at low frequency is attributed to the domain wall displacement. The absorption at highest frequency is attributed to the rotational resonance of domains in the combined anisotropy and demagnetizing fields [25]. Real part of permeability is dependent on many parameters such as stoichiometry, grain structure, composition, impurity contents, saturation magnetization, magnetostriction, crystal anisotropy and porosity [26]. Higher permeability's are favored by large grain size, high saturation magnetization, low porosity, low crystal anisotropy, low magnetostriction and high purity of the material, in particular for small grain sizes; the real permeability depends on grain size [27]

Frequency dependence of imaginary part of permeability (μ'') shows that the values of μ'' for all the ferrites are gradually increased with frequency and shows a maximum at a certain frequency. This feature is well known as natural resonance [28,29]. The permeability of ferrite is correlated to two different magnetizing mechanisms: spin rotation and domain wall motion [30–32]. The decreased value of μ'' at lower frequency and constant at

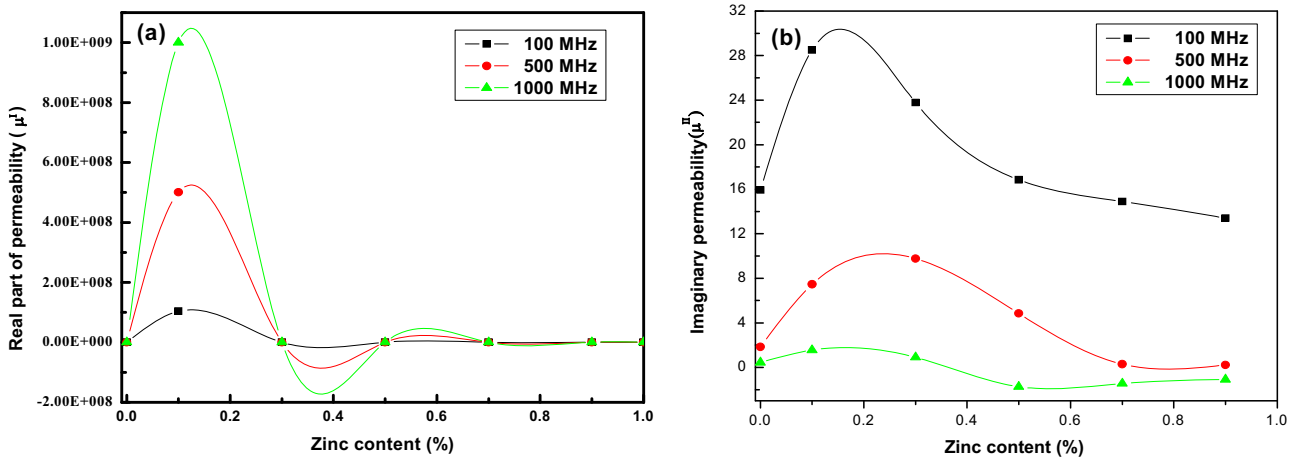

Fig. 6. Compositional dependence of the (a) real part of permeability and (b) imaginary part of permeability at selected frequency for $Mn_{1-x}Zn_xFe_2O_4$ (x=0, 0.1, 0.3, 0.5, 0.7, 0.9 and 1.0).

higher frequency upto 300 MHz is may be due to the contribution of domain wall motion. The compositional dependence of real and imaginary part of permeability, at selected frequency at room temperature is shown in Fig. 6(a) and (b). It could be seen that μ' and μ'' sharply are found to increase, attain maxima with further increase in frequency and decreases with zinc content due to disappearance of pores due to the densification leads to increase of μ' for the present ferrites.

4. Conclusions

Nanocrystalline Mn–Zn ferrites were successfully synthesized by solution combustion method using mixture of fuels (urea and glucose). The effect of Zinc substitution on structural and magnetic properties of Mn–Zn ferrites have been studied at room temperature. The X-ray Diffractometer reveals the formation of spinal cubic structure with an average crystallite size 25–30 nm. The TEM image confirms the synthesized powder are in nanosize from the VSM we observed saturation magnetization, remanance magnetization and magneton number is decreases gradually with increasing Zn^{2+} concentration. The small values of remanance ratio and magneton number suggest the existence of multi domain particles in the samples. The small values of coercivity indicate that the synthesized ferrites can be used low and high frequency applications.

References

[1] P. Hu, H.B. Yang, D.A. Pan, H. Wang, J.J. Tian, S.G. Zhang, X.F. Wang, A. A. Volinsky, J. Magn. Magn. Mater. 322 (2010) 173–177.
[2] U. Ghazanfar, S.A. Siddiqi, G. Abbas, Mater. Sci. Eng. B 118 (2005) 84.
[3] G. Ott, J. Wrba, R. Lucke, J. Magn. Magn. Mater. 535 (2003) 254–255.
[4] H. Waqus, A.H. Quresghi, J. Ther. Anal. Calor 98 (2009) 355.
[5] A.D.P. Rao, B. Ramesh, P.R.M. Rao, S.B. Raju, Il Nuovo Cimento Febbraio 20D (2) (1998).
[6] H.N. Ji, Z.W. Lan, Z. Yu, Y.J. Zhi, Z. Liu, IEEE Appl. Super Electron. Device (2009) 25.
[7] M.J. NasrIsfahani, M. Myndyk, Magnetic properties of nanostructured MnZn ferrite, J. Magn. Magn. Mater. 321 (2009) 152–156.
[8] D. Varshney, K. Verma, A. Kumar, Structural and vibrational properties of $Zn_x Mn_{1-x}Fe_2O_4$ (x=0.0, 0.25, 0.50, 0.75, 1.0) mixed ferrites, Mater. Chem. Phys. 131 (2011) 413–419.
[9] D. Zhang, X. Zhang, et al., Low-temperature fabrication of $MnFe_2O_4$ octahedrons:magnetic and electrochemical properties, Chem. Phys. Lett. 426 (2006) 120–123.
[10] P. Hu, H. Yang, et al., Heat treatment effects on microstructure and magnetic properties of Mn–Zn ferrite powders, J. Magn. Magn. Mater. 322 (2010) 173–177.
[11] C.C. Agrafiotis, V.T. Zaspalis, Self-propagatinghigh temperature synthesis of MnZn-ferrites for inductor applications, J. Magn. Magn. Mater. 283 (2004) 364–374.
[12] K. Praveena, K. Sadhana, S. Bharadwaj, S.R. Murthy, J. Magn. Magn. Mater. 321 (2009) 2433.
[13] Ming-Ru Syue, Fu-Jin Wei, Chan-Shin Chou, Chao-Ming Fu, Thin Solid Films 519 (2011) 8303.
[14] A. Mali, A. Ataie, J. Alloy. Compd. 399 (2005) 245.
[15] Sangeeta Thakur, S.C. Katyal, M. Singh, J. Magn. Magn. Mater. 321 (2009) 1.
[16] L. Neel, Proce. Phys. Soc. Lond. A-65 (1952) 13584.
[17] M. Garcia Del Muro, X. Batlle, A. Labarta, Phys. Rev. B 59 (1999) 13584.
[18] K.J. Standley, Oxide Magnetic Materials, Clarendon Press, Oxford, 1972.
[19] H. Shokrollahi, K. Janghorban, Mater. Sci. Eng. B 141 (2007) 91.
[20] D.J. Craik, Magnetic Oxides, Part 1, Wiley, New York, 1975.
[21] P. Yaseneva, M. Bowker, G. Hutchings, Phys. Chem. Chem. Phys. 13 (2011) 18609.
[22] Song Jie, Wang Lixi, Xu Naicen, Zhang Qitu, J. Rare Earths 28 (3) (2010) 451.
[23] K. Praveena, S.R. Murthty, Mater. Res. Bull. 48 (2013) 4826–4833.
[24] R.V. Mangalaraja, S. Ananthakmar, P. Manohara, F.D. Gnanama, M. Awano, Mater. Sci. Eng. A 367 (2004) 301.
[25] R.B. Pujar, S.N. Kulkarni, C.B. Bellad, B.K. Chougule, J. Mater. Sci. Lett. 16 (1997) 668.
[26] T. Pannaprayil, R. Marande, S. Komarneni, J. Appl. Phys. 69 (8) (1991) 5349.
[27] P.J. Van der Zaag, M.T. Johnson, J.J.M. Ruigrok, C. Bordel, H.J. de Wit, J. Magn. Magn. Mater. 129 (1994) L137.
[28] J. Smit, H.P.J. Wijn, Ferrites, Phillips Technical Library, Eindhoven, The Netherlands (1959), p. p134.
[29] I.L. Snoek, Physica 4 (1948) 207.
[30] A.K.M. Akther Hossain, K. Khirul Kabir, M. Seki, T. Kawai, H. Tabata, J. Phys. Chem. Solids (2007) 1933.
[31] A.K.M. Akther Hossain, H. Tabata, T. Kawai, J. Magn. Magn. Mater. 320 (2008) 1157.
[32] K. Sun, Z.W. Lan, Z. YU, L.Z. Li, H.N. Ji, Z.Y. Xu, Mater. Chem. Phys. 113 (2009) 788.